# On Beam Widening for RIS-Assisted Communications Using Genetic Algorithms

Maarouf Al Hajj, Khaled Tahkoubit, Hmaied Shaiek, Valéry Guillet, Didier Le Ruyet

▶ **To cite this version:**

Maarouf Al Hajj, Khaled Tahkoubit, Hmaied Shaiek, Valéry Guillet, Didier Le Ruyet. On Beam Widening for RIS-Assisted Communications Using Genetic Algorithms. 2023 Joint European Conference on Networks and Communications & 6G Summit (EuCNC/6G Summit), Jun 2023, Gothenburg, Sweden. pp.24-29, 10.1109/EuCNC/6GSummit58263.2023.10188311 . hal-04272973

**HAL Id: hal-04272973**

**https://cnam.hal.science/hal-04272973v1**

Submitted on 9 Oct 2024

**HAL** is a multi-disciplinary open access archive for the deposit and dissemination of scientific research documents, whether they are published or not. The documents may come from teaching and research institutions in France or abroad, or from public or private research centers.

L'archive ouverte pluridisciplinaire **HAL**, est destinée au dépôt et à la diffusion de documents scientifiques de niveau recherche, publiés ou non, émanant des établissements d'enseignement et de recherche français ou étrangers, des laboratoires publics ou privés.

# On Beam Widening for RIS-Assisted Communications Using Genetic Algorithms

Maarouf Al Hajj*, Khaled Tahkoubit§, Hmaied Shaiek§, Valéry Guillet* and Didier Le Ruyet§
* Orange Labs, France
§ Conservatoire National des Arts et Métiers (CNAM), France
Emails:{maarouf.alhajj, valery.guillet}@orange.com, {khaled.tahkoubit, hmaied.shaiek, didier.le_ruyet}@lecnam.net

***Abstract*—As future wireless communication systems aim to achieve increased data rates, system capacity, and reduced latency and power consumption, they have shifted towards higher frequency bands such as Millimeter Wave (mmWave) and Terahertz spectrums. However, these spectrums pose challenges in terms of the quality of the communication link, including large path-loss and limited coverage, as well as difficulties in system and antenna design. Reconfigurable Intelligent Surfaces (RISs) have recently been proposed as a promising low-cost and low-power consumption solution to enhance the performance of wireless communication systems. However, beamforming with RISs can be difficult, especially in the presence of beam widening requirements, which aim to produce wide beams for cell or sector-wide broadcasting, among other applications. In this paper, a new approach for beam widening in RIS-assisted communications using genetic algorithms is proposed. The focus is on using phase-only tapering to achieve wide beams while minimizing sidelobes (SSL) and beam ripple. To address this problem, two cost functions are developed and optimized using genetic algorithms. The optimization results in a codebook of 1-bit phase patterns with varying beamwidths, making it possible to widen the beams without requiring extra controllers or specific element designs. The proposed approach is evaluated through simulation results, which demonstrate its effectiveness in achieving wide beams while maintaining a low level of sidelobes and beam ripple.**

## I. Introduction

Seeking increased data rates and system capacity, and also decreased latency and power consumption, future wireless communication systems have shifted towards higher frequency bands like Millimeter Wave and Terahertz spectrums. These spectrums, while providing the much-needed large available bands, have their drawbacks on the quality of the communication link, like large path-loss and limited coverage, in addition to challenges in system and antenna design. Multiple solutions, like Ultra-Massive multiple-input multiple-output (MIMO) and reflectarrays/transmitarrays, have being investigated as solutions to the path-loss problems in high-frequency bands [1]. Transmitarrays and reflectarrays are a subset of the much promising technology of reconfigurable intelligent surface (RIS)s that has less cost and power consumption in comparison with fully digital massive MIMO solutions. Instead of modifying the channel, transmitarrays and reflectarrays act as antennas with many reconfigurable elements. Antennas with a large number of elements allows focusing the radiated energy in a specific direction of space, producing very narrow, highly directive beams that can counter the propagation path loss. However, as shown in [2], narrow beams tend to be more susceptible to blockage. They may also increase overhead by virtue of longer sweeping times, and are more susceptible to pointing errors due to user mobility [3].

To overcome these limitations, research is being conducted on beam widening techniques for large-array antennas like massive MIMO. The goal is to obtain a wide beam that can be used for cell or sector-wide broadcasting, among other applications. A discussion over where a wide beam could be formed using massively large antenna arrays took place in RAN1#87, and in [3] some examples have been given on wide beamforming using massive arrays. By increasing the number of antenna elements, the antenna arrays' beams get narrower [4], increasing their directivity. This has prompted the development of different techniques for beam-widening like in [5], [6] and [7] which allowed for variation in the element amplitudes, and in [8] and [4] where only the element phases were optimized while their amplitudes stayed constant. However, since beam widening results in reduced antenna gain, it should be only used when it leads to improved performance.

Generally, there have been two approaches to beam widening, either by amplitude tapering or by phase tapering. Tapering is generally defined as the manipulation of the amplitude contribution of an individual element to the overall antenna response [9]. Amplitude tapering, in its extreme, will lead to only one transmitting element being active, and while this produces the widest beam, it is not at all efficient in terms of output power [3] due to the poor utilization of power amplifiers in active antennas and in the context of passive antenna arrays, like transmitarrays, losing energy otherwise propagated through the elements. Phase tapering, on the other hand, aims to widen the transmitted beam by only changing the phases at the transmitting elements. The downside of phase tapering is that it will introduce some level of spatial beam ripple. While a combination of both amplitude and phase tapering methods can be used to ensure an acceptable level of resource utilization, phase-only tapering techniques seem to be more attractive.

In this paper, we develop an optimization method, based on the genetic algorithm (GA), allowing the generation of a codebook with wide beams by phase-only tapering of a 1-bit coded transmitarray antenna, while ensuring the minimum level of sidelobes and beam ripple. The rest of this paper is structured as follows. In section II, we will present the system model, as well as some fundamental concepts. Then, we will propose, in section III, two optimization algorithms allowing to have an advanced control of the widths of the beams. Section IV will give some simulation results comparing the two proposed optimization approaches before a general conclusion.

## II. System model

Fig. 1, presents a general RIS-assisted single-input single output (SISO) wireless communication system in a transmit-array (TA) scenario. In this figure a meta-surface, with $M \times N$ unit-cells (UCs), is positioned in the plane $[O, x, y]$. These UCs are spaced by a distance $d_x$, along the $[O, x)$ axis and $d_y$, along the $[O, y)$ axis. We note $D = \max(M \times d_x, N \times d_y)$. In this study, we consider a square-shaped RIS with size $M = N = 20$ operating in 26 $GHz$ frequency band. For inter-UC spacing, we consider $d_x = d_y = \lambda/2$, where $\lambda$ is the wavelength. The transmitting horn antenna is located on the negative $Z$ axis, at a focal distance $F$. This distance is a function of $D$ and of the radiation patterns of the horn antennas used [10]. When using one horn antenna, the optimal value of $F/D$ is equal to 0.47 for a square array of $20 \times 20$ UCs. In Fig. 1, we can distinguish the definitions of the different angles for the transmitting/receiving antennas and also for the unit cells of the RIS : In this figure, $\theta^{tx}_{mn}$ and $\theta^{rx}_{mn}$ represent the angle from the normal of the unit cell $(m, n)$ to the transmitting and receiving antennas, respectively.

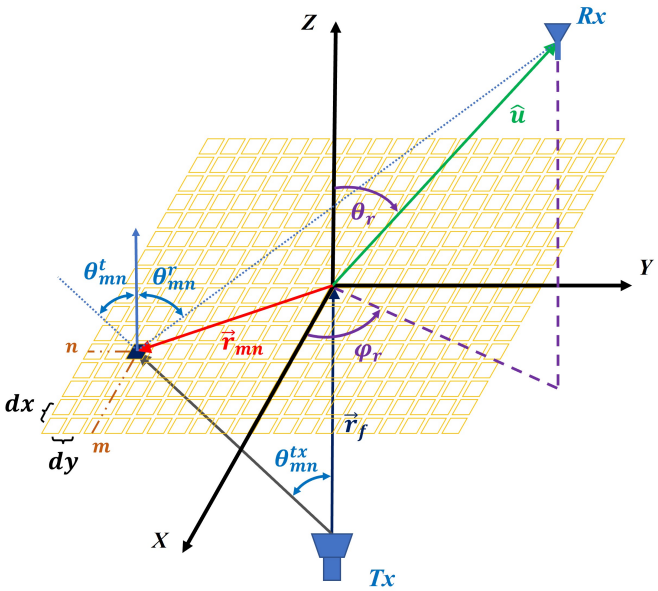


Fig. 1: An illustration of the transmitarray's system model.

We assume a cosine $q$ model for the Tx and the UCs. The Tx radiation pattern can be expressed as

$$F^{tx}(\theta^{tx}_{mn}) = \cos^4(\theta^{tx}_{mn}), \tag{1}$$

where $\theta^{tx}_{mn}$ is the angle between the Tx and the normal of the $(m, n)^{th}$ UC. Moreover, the UCs consist of a phase shifting section connected to Rx and Tx radiating elements. Each element is modeled as a uniform aperture whose radiation pattern, in transmission and reception, is given by

$$F^{x}(\theta^{x}_{mn}) = \frac{4\pi A_{phy}}{\lambda^2} cos(\theta^{x}_{mn}), \tag{2}$$

with $x \in \{t, r\}$ for transmission/reception, and where $A_{phy}$ is the physical area of the unit cell, and $\theta^{x}_{mn}$ is the angle between the normal to the UC and the Tx or the Rx. Table I summarizes the general parameters to be used in our system model.

| | |
|---|---|
| Frequency | $f_c$ = 26 GHz |
| Wavelength | $\lambda = c/f_c$ |
| Number of UCs | $N \times M = 20 \times 20$ |
| UCs spacing | $d_y = d_x = \lambda/2$ |
| Optimum $F/D$ ratio | 0.47 |

TABLE I: System model general parameters

The boundary between the far field and the near field of the antenna array is defined as $L = 2D^2/\lambda$. When the distance between the transmitter/receiver and the center of the RIS is less than $L$, the transmitter/receiver are considered to be in the near field of the RIS. Otherwise, they are in the far field of the RIS. It is worth noting that when the transmitter is replaced by a receiver, the above definition remains the same due to the reciprocity of the antenna array.

Considering the RIS configurations depicted in Fig. 1, the analytical expression for the far field radiated at a given direction $(\theta_r, \varphi_r)$ is given as [11]

$$E(\theta_r, \varphi_r) = \sum_{m=1}^{M}\sum_{n=1}^{N} F^{tx}(\theta^{tx}_{mn}) \times \frac{F^{t}(\theta^{t}_{mn})}{\|\vec{r}_{mn} - \vec{r}_f\|} e^{-jk(\|\vec{r}_{mn} - \vec{r}_f\| - \vec{r}_{mn}.\hat{u})} \times F^{r}(\theta^{r}_{mn}) e^{j\Phi_{mn}} \tag{3}$$

where $\hat{u}$ is the observation direction, $\vec{r}_f$ is the vector between the Tx and the center of the RIS, $\vec{r}_{mn}$ is the vector between center of the RIS and the UC $(m, n)$, $e^{j\Phi_{mn}}$ is the phase control to be applied to the $(m, n)^{th}$ UC, $k$ is the wavenumber and the operator $\|\cdot\|$ is the norm of a vector.

To speed up the computation of the radiation pattern, we replace the double summation in (3) with an inverse fast Fourier transform (IFFT). Assuming the radiation pattern for a unit cell on the transmitting side in the far-field given by equation (2), the spectral function on a discrete set of angular coordinates [12] is given by

$$E(u, v) = (1 - u^2 - v^2)^{1/2} M.N \times \text{IFFT}\left[\frac{F^{tx}(\theta^{tx}_{mn}) F^{t}(\theta^{t}_{mn})}{\|\vec{r}_{mn} - \vec{r}_f\|} \times e^{j\Phi_{mn} - jk\|\vec{r}_{mn} - \vec{r}_f\|}\right], \tag{4}$$

where

$$u = \sin(\theta_r)\cos(\phi_r) = \frac{2\pi}{N^{FFT}_x d_x k} p, \tag{5}$$

and

$$v = \sin(\theta_r)\sin(\phi_r) = \frac{2\pi}{N^{FFT}_y d_y k} q, \tag{6}$$

are the angular coordinates of the radiation pattern, with $N^{FFT}_x$ and $N^{FFT}_y$ being the output shape of the FFT in the $x$ and $y$ directions respectively[1], and $p = 0, 1, 2, ..., N^{FFT}_x$

[1] If $N^{FFT}_x$ and $N^{FFT}_y$ are bigger than $N$ and $M$, the input to the FFT is zero-padded to reach the specified axis lengths.

and $q = 0, 1, 2, ...N_y^{FFT}$. Assuming an infinite array approach [13], we can express the phase matrix required to set the main beam in the $(\theta_r, \varphi_r)$ direction by

$$\Phi_{mn} = -k(m.d_x \sin\theta_r \cos\varphi_r + n.d_y \sin\theta_r \cos\varphi_r) \quad (7)$$

Once the radiation pattern is calculated, the RIS's directivity can be obtained using

$$D = \frac{4\pi \left|E(\theta_r, \varphi_r)\right|^2}{\int_0^{2\pi}\int_0^{\pi} \left|E(\theta, \varphi)\right|^2 \sin\theta \, d\theta \, d\varphi}, \quad (8)$$

where $\theta_r$ and $\varphi_r$ are the angular directions of the main beam. Since the radiation pattern can be expressed in the angular coordinates $(u, v)$ (given by (4)) instead of the spherical coordinates $(\theta, \phi)$, we can express the directivity in the former coordinate system as [14]

$$D = \frac{4\pi \left|E(u_r, v_r)\right|^2}{\iint\limits_{u^2+v^2\leq 1} \left|E(u, v)\right|^2 \, d\Omega} \quad (9)$$

where $d\Omega$ is the beam solid angle in the angular coordinates. It is expressed as

$$d\Omega = \frac{du \, dv}{\sqrt{1 - (u^2 + v^2)}}, \quad (10)$$

which is computed numerically.

## III. Optimization Problem Formulation

In this section, we will introduce two GA-based algorithms for optimizing the phase grid to get a radiation pattern with specific constraint on the Side-Lobe Level (SLL) and the Half-Power Beam-Width (HPBW) of the designed beams. The SLL is defined as the maximum value of the normalized radiation pattern outside the main beam, and the HPBW is the width, in degrees, of the main lobe at $\max(E(u, v)) - 3$ dB. The first approach is a straightforward one that is used as a baseline for comparison with the second approach.

The objective function optimized by the GA algorithm can be the antenna gain in a given direction or the difference between the obtained and desired radiated field. The initial population is composed of a set of $W = M \times N$ random binary matrices (chromosomes). At each iteration we apply selective reproduction, crossover, mutation as following [15]:

**Selection:** The $W_b$ chromosomes that have the lowest fitness are discarded. The remaining $W - W_b$ chromosomes are applied to the crossover and mutation processes and are then selected for the new population. The best $W_b$ chromosomes are directly added to the new population without applying any processing.
**Crossover:** The probability of crossover is set to $P_c$ and $W_c = (W - W_b) \times P_c$ chromosomes are applied to the crossover and then passed to the new population. The remaining $(W - W_b) \times (1 - P_c)$ chromosomes are directly passed to the new population. We have implemented the two-points crossover method, where two crossover points are chosen randomly from the parent chromosomes. The bits between the two points are then swapped between the parent chromosomes.
**Mutation:** The probability of mutation is set to $P_m$ and after the crossover process $W_m = (W - W_b) \times P_m$ chromosomes are applied to the mutation and added to the new population. The remaining $(W - W_b) \times (1 - P_m)$ chromosomes are directly added to the new population without any mutation.

### A. First optimization approach

The cost function to be minimized by the GA algorithm can be written as a sum of two sub-functions $\psi_1$ and $\psi_2$. The first sub-function $\psi_1$ aims to maximize the field in the beamforming directions while controlling the HPBW, while $\psi_2$ controls the SLL. The global cost function related to this first optimization approach is given by

$$\Psi^{(1)} = \psi_1 + \psi_2, \quad (11)$$

with

$$\psi_1 = \sum_{(\theta_i, \varphi_j) \in S_P} \left(E(\theta_i, \varphi_j) - V\right)^2, \quad (12)$$

and

$$\psi_2 = \max_{(\theta_n, \varphi_r) \in S_C} \left( \left(E(\theta_n, \varphi_r) - (V - \beta)\right)^2 \right), \quad (13)$$

where the sets $S_P$ and $S_C$ contain the coordinates of the pointing directions and the directions where we want to control the SLL, respectively. $V$ is the maximum field obtained after phase compensation over the two states of the one bit-coded phase on each UC, and $\beta$ is the target radiation pattern value outside the main beam. We set the population size to $W = 36$, the number of generations is set to $G = 1000$, and $W_b = 6$ elements will be discarded in each generation. The crossover probability is set to $P_c = 0.8$ and the mutation probability has multiple values: $P_m = 0.1, 0.2, 0.4$, and $0.5$.

### B. Second optimization approach

In this approach, we aim to improve upon the first, by better defining the areas of interest for the optimization, and by balancing the weights of the SLL and the HPBW regions. We also change the parameters of the GA to adapt to the new approach. The objective function to be minimized is chosen as the difference between the normalized radiation pattern of the antenna surface and the pre-defined performance metrics. However, since we are mainly concerned with the SLL, and the HPBW, we limit the contribution to the objective function to only the relevant areas of the radiation pattern specified by an upper mask $M_U$ and a lower mask $M_L$. This objective function is defined as

$$\Psi^{(2)} = \sum_{(u,v) \in S_L} \left( \frac{\hat{E}(u, v) - M_L(u, v)}{|S_L|} \right)^2 + \sum_{(u,v) \in S_U} \left( \frac{\hat{E}(u, v) - M_U(u, v)}{|S_U|} \right)^2, \quad (14)$$

where

$$S_L = \left\{ (u, v) \mid \hat{E}(u, v) < M_L(u, v) \right\}, \quad (15)$$

$$S_U = \left\{ (u, v) \mid \hat{E}(u, v) > M_U(u, v) \right\}, \quad (16)$$

and $|\cdot|$ denotes the cardinality of a set. In this approach, the sidelobes contribute to $\Psi^{(2)}$ only when it is higher than $M_U$. This makes it so that the algorithm does not aim to

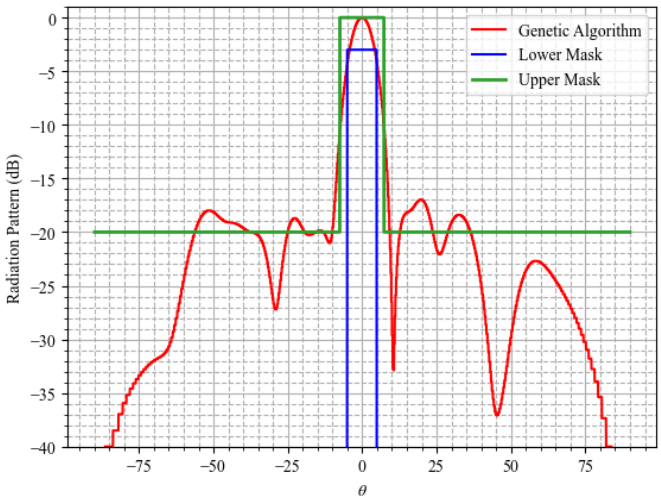


Fig. 2: An example of the lower mask, upper masks, and the resulting radiation pattern along $\theta$ generated by the GA.

approach the sidelobes to the target value, but only to decrease it. The same logic also applies to the main beam. $M_L$ and $M_U$ are defined as circular in the $(u, v)$ plane, and are defined as follows

$$M_L(u,v) = \begin{cases} \min(\hat{E}(u,v)) & \text{for} \quad \mathcal{E}_L(u,v;\Theta_t) > 1 \\ -3 & \text{for} \quad \mathcal{E}_L(u,v;\Theta_t) \leq 1 \end{cases}, \quad (17)$$

and

$$M_U(u,v) = \begin{cases} \tau & \text{for} \quad \mathcal{E}_U(u,v;\Omega_t) > 1 \\ 0 & \text{for} \quad \mathcal{E}_U(u,v;\Omega_t) \leq 1 \end{cases}, \quad (18)$$

where

$$\mathcal{E}(u,v;\alpha) = (u-u_0)^2 + (v-v_0)^2 - \sin^2\alpha, \quad (19)$$

$\Theta_t$ and $\Omega_t$ are the target HPBW and first-null beamwidth (FNBW) of the beam, respectively, and $\tau$ is the target SLL. $u_0$ and $v_0$ are the coordinates of the beam's direction in the $(u, v)$ plane, respectively. $\hat{E}(u, v)$ is the normalized radiation pattern of the surface after each generation, based on the surface's phase matrix, $\Phi_{mn} \in \{0, \pi\}$, generated by the optimization algorithm. An example of the lower and upper masks is presented in Fig. 2. We use Gaussian mutation with $P_m = 0.1$, binomial crossover with 0.5 bias, 2 offsprings, and $P_c = 0.9$, binary tournament selection, and Latin hypercube sampling.

## IV. Simulation Results

In this section, we present the simulation results of the analytical approach to beamforming, in addition to the optimization approaches presented in the previous section. For each resulting phase matrix and radiation pattern, we determine the SLLs and the HPBWs in the 3D plane instead of in a 2D slice like most studies, which is not at all sufficient in evaluating the quality of the optimization. We use the same parameters as described previously. We also choose the value of $\tau = -30$ in (18), and while we never really achieve this level of SLL, it is what gives us the best results in most cases. Moreover, in the second approach, we use the Unified Non-dominated Sorting Genetic Algorithm III (U-NSGA-III) algorithm [16] implemented in the open source framework for multi-objective optimization in Python, pymoo [17].

| $\theta_r$ | $\Theta(^\circ) : (\theta, \varphi)$ | SLL(dB) | $D$(dbi) |
|---|---|---|---|
| 0° | (7.0,7.0) | -16.96 | 26.13 |
| 20° | (7.3, 6.9) | -14.07 | 25.35 |
| 40° | (8.9, 7.3) | -15.58 | 25.05 |
| 60° | (12.1, 6.7) | -8.35 | 21.25 |

TABLE II: Beamwidths, SLL, and directivity for analytically computed phases.

In table II we present the radiation pattern characteristics of the analytical phase calculation, and in tables III and IV, the performance of the two optimization approaches, is compared in terms of their resulting HPBWs, SLLs, and directivities $D$, for different steering angles $\theta_r$ from the normal. We notice that the GA can produce radiation patterns with lower levels of SLL, and higher directivity, than the analytical method, especially at larger steering angles. Moreover, we can see the expected drop in directivity, and the increase in SLL with the increase of the steering angle $\theta_r$ and the target HPBW, $\Theta_t$. The results show good performance of the approaches, especially the second, even with 1-bit quantization of the phases. It also shows the increase in the $\theta$ dimension of the main beam for the second approach for larger steering angles, similar to the analytical method, due to the circular masks in the $(u, v)$ plane.

Fig. 3 shows the phase matrices resulting from the first and second approaches, for a beam with target HPBW, $\Theta_t = 20^\circ$ in the broadside direction and at $\theta_r = 40^\circ$. We can see that, while the second approach produces a fairly regular phase grid in the broadside direction, the same cannot be said for the steered scenario. This irregularity is a result of the attempt to reduce the level of peaks in the off-main-beam direction. Since the first approach has less SLL and HPBW control, the resulting grid is more regular.

In Fig. 4, the far-field radiation patterns of the phase matrices are shown. The second approach has a more uniform radiation pattern than the first approach for both the broadside and the steered scenarios, which does not respect the target HPBW to reduce the SLL. This is due to the better control of the SLL and the HPBW provided by the second approach's cost function. Moreover, the second approach prioritizes having low SLL to having more nulls outside the main beam.

## V. Conclusion

In this paper, we have proposed two optimization approaches, based on genetic algorithms, which allow generating wide beams while controlling the SLL. With the first optimization approach, the cost function maximizes the radiated field in the steering direction while keeping the 3D SLL close to a target value. With the second approach, two masks: upper and lower are introduced in a new cost function to minimize the SLL while respecting a specific HPBW. The simulation results show the supremacy of the second approach to achieve consistently wide beams with well-controlled SLLs, even out-of the broadside.

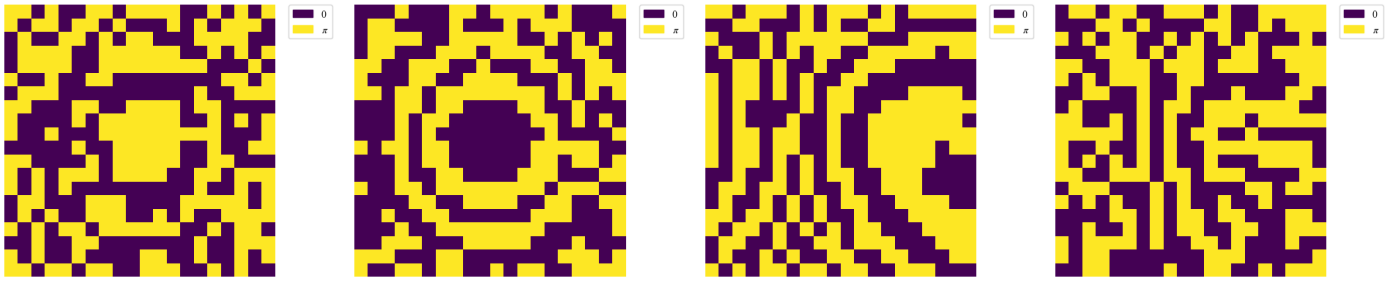


(a) (b) (c) (d)

Fig. 3: Phase grids for the broadside beam obtained from (a) the first and the (b) second optimization approaches, and for the beam with $\theta_r = 40°$ from (c) the first and (d) the second approaches.

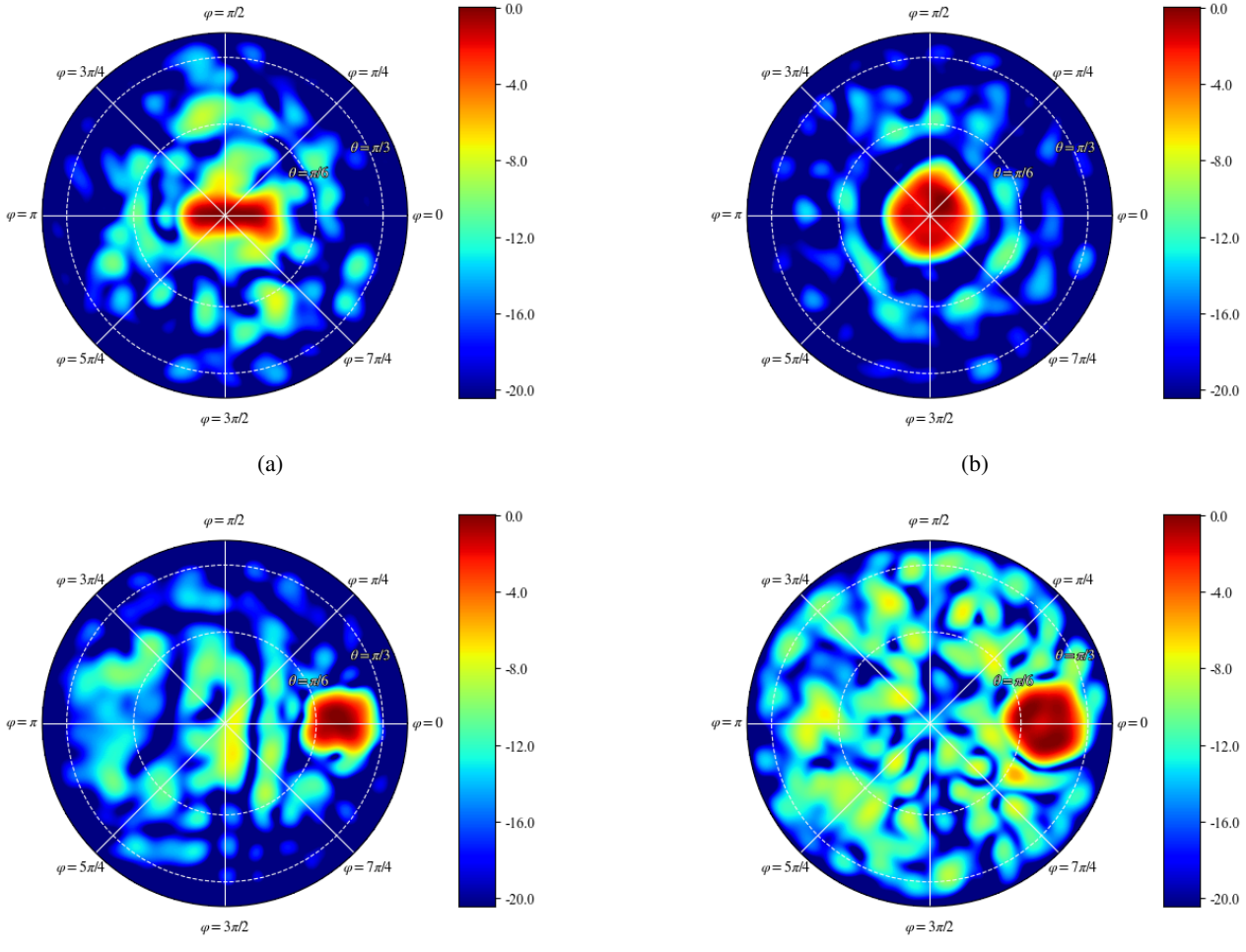


(a) (b) (c) (d)

Fig. 4: Normalized radiation patterns for the broadside beam obtained from (a) the first and (b) the second optimization approaches, and for the beam with $\theta_r = 40°$ from (c) the first and (d) the second approaches.


## ACKNOWLEDGMENT

This work has been done in context of the MESANGES Project ANR-20-CE25-0016-01.

| $\theta_r$ | $\Theta_t = 6°$ | | | $\Theta_t = 10°$ | | | $\Theta_t = 20°$ | | |
|---|---|---|---|---|---|---|---|---|---|
| | $\Theta(°)$: $(\theta, \varphi)$ | SLL (dB) | $D$ (dBi) | $\Theta(°)$: $(\theta, \varphi)$ | SLL (dB) | $D$ (dBi) | $\Theta(°)$: $(\theta, \varphi)$ | SLL (dB) | $D$ (dBi) |
| $0°$ | (7.8, 14.2) | -7.67 | 20.64 | (7.7, 14.9) | -12.08 | 22.49 | (9.0, 28.1) | -7.43 | 18.91 |
| $20°$ | (9.0, 11.4) | -8.80 | 21.59 | (9.8, 12.8) | -7.99 | 20.34 | (10.1, 20.1) | -9.66 | 20.27 |
| $40°$ | (9.4, 9.9) | -7.79 | 20.67 | (10.9, 12.5) | -5.46 | 19.35 | (13.8, 16.0) | -6.89 | 18.69 |
| $60°$ | (8.7, 10.8) | -7.13 | 19.45 | (9.0, 11.6) | -6.87 | 19.27 | (9.5, 17.8) | -5.07 | 18.01 |

TABLE III: Table showing the beamwidths and SLLs resulting from the first optimization approach (III-A) for different steering angles.

| $\theta_r$ | $\Theta_t = 6°$ | | | $\Theta_t = 10°$ | | | $\Theta_t = 20°$ | | |
|---|---|---|---|---|---|---|---|---|---|
| | $\Theta(°)$: $(\theta, \varphi)$ | SLL (dB) | $D$ (dBi) | $\Theta(°)$: $(\theta, \varphi)$ | SLL (dB) | $D$ (dBi) | $\Theta(°)$: $(\theta, \varphi)$ | SLL (dB) | $D$ (dBi) |
| $0°$ | (6.9, 7.0) | -17.91 | 26.33 | (9.3,9.4) | -16.99 | 24.11 | (18.3, 20.8) | -7.25 | 16.94 |
| $20°$ | (7.1, 7.1) | -16.80 | 26.04 | (10.8, 11.5) | -13.31 | 22.04 | (21.3, 23.0) | -7.17 | 17.14 |
| $40°$ | (8.6, 6.9) | -16.12 | 25.18 | (10.1,8.9) | -15.88 | 23.11 | (20.8, 21.0) | -6.05 | 16.21 |
| $60°$ | (11.7, 7.2) | -12.14 | 23.13 | (17.6, 11.1) | -9.89 | 19.35 | - | - | - |

TABLE IV: Table showing the beamwidths and SLLs resulting from the second optimization approach (III-B) for different steering angles.

## REFERENCES


[1] I. F. Akyildiz, C. Han, and S. Nie, "Combating the distance problem in the millimeter wave and terahertz frequency bands," *IEEE Communications Magazine*, vol. 56, no. 6, pp. 102–108, Jun. 2018, ISSN: 1558-1896. DOI: 10.1109/MCOM.2018.1700928.

[2] G. R. MacCartney, T. S. Rappaport, and S. Rangan, "Rapid Fading Due to Human Blockage in Pedestrian Crowds at 5G Millimeter-Wave Frequencies," in *GLOBECOM 2017 - 2017 IEEE Global Communications Conference*, Dec. 2017, pp. 1–7. DOI: 10.1109/GLOCOM.2017.8254900.

[3] Ericsson, "On Forming Wide Beams," 3GPP R1-1700772, Jan. 20, 2017.

[4] Intel, "Codebook With Beam Broadening," 3GPP R1-1611929, Nov. 18, 2016.

[5] C. Zhang, Y. Huang, Y. Jing, and L. Yang, "Energy Efficient Beamforming for Massive MIMO Public Channel," *IEEE Transactions on Vehicular Technology*, vol. 66, no. 11, pp. 10 595–10 600, Nov. 2017, ISSN: 1939-9359. DOI: 10.1109/TVT.2017.2756994.

[6] V. Raghavan, J. Cezanne, S. Subramanian, A. Sampath, and O. Koymen, "Beamforming Tradeoffs for Initial UE Discovery in Millimeter-Wave MIMO Systems," *IEEE Journal of Selected Topics in Signal Processing*, vol. 10, no. 3, pp. 543–559, Apr. 2016, ISSN: 1941-0484. DOI: 10.1109/JSTSP.2016.2523442.

[7] W. Fan, C. Zhang, and Y. Huang, "Flat Beam Design for Massive MIMO Systems via Riemannian Optimization," *IEEE Wireless Communications Letters*, vol. 8, no. 1, pp. 301–304, Feb. 2019, ISSN: 2162-2345. DOI: 10.1109/LWC.2018.2871260.

[8] K. H. Sayidmarie and Q. H. Sultan, "Synthesis of wide beam array patterns using random phase weights," in *2013 International Conference on Electrical Communication, Computer, Power, and Control Engineering (ICECCPCE)*, Dec. 2013, pp. 52–57. DOI: 10.1109/ICECCPCE.2013.6998734.

[9] P. Delos, B. Broughton, and J. Kraft, "Phased-array antenna patterns (part 6)-sidelobes and tapering," *Microwaves&RF*, 2020.

[10] A. Clemente, L. Dussopt, R. Sauleau, P. Potier, and P. Pouliguen, "Focal Distance Reduction of Transmit-Array Antennas Using Multiple Feeds," *IEEE Antennas and Wireless Propagation Letters*, vol. 11, pp. 1311–1314, 2012, ISSN: 1548-5757. DOI: 10.1109/LAWP.2012.2227105.

[11] P. Nayeri, *Advanced Design Methodologies and Novel Applications of Reflflectarray Antennas*. Ph. D dissertation, University of Mississippi, 2012.

[12] T. Shan, X. Pan, M. Li, S. Xu, and F. Yang, "Coding Programmable Metasurfaces Based on Deep Learning Techniques," *IEEE Journal on Emerging and Selected Topics in Circuits and Systems*, vol. 10, no. 1, pp. 114–125, Mar. 2020, ISSN: 2156-3365. DOI: 10.1109/JETCAS.2020.2972764.

[13] B. Diamond, "A generalized approach to the analysis of infinite planar array antennas," *Proceedings of the IEEE*, vol. 56, no. 11, pp. 1837–1851, Nov. 1968, ISSN: 1558-2256. DOI: 10.1109/PROC.1968.6758.

[14] W. P. M. N. Keizer, "APAS: An Advanced Phased-Array Simulator," *IEEE Antennas and Propagation Magazine*, vol. 52, no. 2, pp. 40–56, Apr. 2010, ISSN: 1558-4143. DOI: 10.1109/MAP.2010.5525565.

[15] J. H. Holland, "Genetic algorithms," *Scientific american*, vol. 267, no. 1, pp. 66–73, 1992.

[16] N. Hansen and A. Ostermeier, "Completely Derandomized Self-Adaptation in Evolution Strategies," *Evolutionary Computation*, vol. 9, no. 2, pp. 159–195, Jun. 2001, ISSN: 1063-6560. DOI: 10.1162/106365601750190398.

[17] J. Blank and K. Deb, "Pymoo: Multi-Objective Optimization in Python," *IEEE Access*, vol. 8, pp. 89 497–89 509, 2020, ISSN: 2169-3536. DOI: 10.1109/ACCESS.2020.2990567.